73rd International Astronautical Congress (IAC), Paris, France, 18-22 September 2022.

IAC-22.A3.IPB.36.x73185

Phase-A Design of a Mars South Pole Exploration Mission: MARS PENGUIN

Francesco Ventre[a*], Nicola Boscolo Fiore[b], Elisa De Astis[c], Vahid Nateghi[d], Claudio Pedrazzini[e], Massimo Piazza[f], Lorenzo Pisani[g], Sabrina Saban[h], Prof. Michèle Lavagna[i]

[a]*Confindustria Brescia, 25124 Brescia, Italy,* ventre@confindustriabrescia.it
[b]*Telespazio s.p.a., 00156 Rome, Italy,* nicola.boscolo@telespazio.com
[c]*Capgemini Engineering, 20154 Milan, Italy,* elisa.deastis@capgemini.com
[d]*Polytechnic University of Milan, 20156 Milan, Italy,* vahid.nateghi@mail.polimi.it
[e]*ENPULSION GmbH, 2700 Wiener Neustadt, Austria,* claudio.pedrazzini@enpulsion.com
[f]*Infinite Orbits, 31000 Toulouse, France,* massimo@infiniteorbits.io
[g]*Dublin City University, D09 E432 Dublin, Ireland,* lorenzo.pisani@dcu.ie
[h]*Polytechnic University of Milan, 20156 Milan, Italy,* sabrina.saban@mail.polimi.it
[i]*Polytechnic University of Milan, 20156 Milan, Italy,* michelle.lavagna@polimi.it
[*]Corresponding author

Abstract

During the last 60 years, several space missions have been designed and launched to explore our neighboring planet, Mars. Most of these expeditions had the goal of mapping the planet and evaluating some of its key characteristics, such as terrain configuration and composition. In this context, in 2018 the Mars Advanced Radar for Subsurface and Ionosphere Sounding (MARSIS) instrument, on board the European Space Agency's (ESA) Mars Express Orbiter, led to the discovery of a subglacial lake located at the South Pole of Mars, in the same area where several geysers were first observed in the late '90s. This discovery suggested complex seasonal dynamics associated with both the Mars icy caps and led to the launch of some missions to inspect the main features in situ. However, none of the attempts was successful. This paper presents the phase-A design of a fully European rover mission, called MARs South Pole ExploratioN and Geysers in-sitU Investigation (MARS-PENGUIN), to sample the icy crust above the South Pole subglacial lake in different locations and characterize the aforementioned geysers' phenomena from a close distance. The mission, composed of a service module, a rover, and a martian helicopter, is designed to reach the subglacial lake region during the martian spring, in 2029, after a ten-month cruise, to spot the geysers during their activity period. This work reports the requirements, the feasibility analysis, and the preliminary technical development for each subsystem. Moreover, the operational phase is characterized, with an emphasis on the sampling strategies adopted to meet the mission objectives.

Keywords: mission, mars, rover, exploration, lake, geysers

Acronyms

BER	Bit Error Rate
ConOps	Concept of Operations
COSPAR	Committee on Space Research
DoF	Degrees of Freedom
EDL	Entry, Descent and Landing
EFPA	Entry Flight Path Angle
EPS	Electric Power Subsystem
FEA	Finite Element Analysis
GNC	Guidance, Navigation & Control
HGA	High Gain Antenna
HiRISE	High Resolution Imaging Science Experiment
JPL	Jet Propulsion Laboratory
LEOP	Launch and Early Orbit Phase
LGA	Low Gain Antenna
LoS	Line of Sight
LVA	Launch Vehicle Adapter
MARSIS	Mars Advanced Radar for Subsurface and Ionosphere Sounding
MAVEN	Mars Atmosphere and Volatile Evolution
MRO	Mars Reconnaissance Orbiter
NAIF	Navigation and Ancillary Information Facility
NASA	National Aeronautics and Space Administration
OBDH	On-board Data Handling
P/L	Payload
RA	Robotic Arm

RLS	Raman Laser Spectrometer
RTG	Radioisotope Thermoelectric Generator
RUHF	Rover Ultra High Frequency
S/C	spacecraft
SNR	Signal-to-Noise Ratio
SOI	Sphere of Influence
SSI	Surface Stereo Imager
TCM	Trajectory Correction Manoeuvre
TCS	Thermal Control Subsystem
TOF	time of flight
TRL	Technology Readiness Level
UHF	Ultra-High Frequency

1. Introduction

Since the beginning of space exploration, Mars is the place in the Solar System in which most missions have been attempted (excluding the Moon). The first ones started in the early 60s, but it was necessary to wait until 1965 for the first successful mission, when the American spacecraft Mariner 4 completed a flyby of the planet. Some of these missions have accomplished their objectives obtaining positive results, as the rover Curiosity which is still operational, whereas others failed.

With the aim of contributing to the future exploration of Mars, in the context of the Space Mission Analysis and Design course at Politecnico di Milano, under the guidance of Professor Michéle Lavagna, the mission presented in this paper was designed. MARS-PENGUIN (MARs South Pole ExploratioN and Geysers in-sitU Investigation) is a mission to visit the Southern Polar Cap of Mars with three main objectives:

- Deepen the knowledge about the seasonal evolution of southern polar caps on Mars;
- Perform in-situ analyses to characterise the region above the sub-glacial lake discovered in the south pole region, and study its interaction with the Martian atmosphere;
- Conduct in-situ prospecting to understand the geyser-like eruption phenomena.

The mission is hereby detailed describing the landing and mining site selection (Section 2.), the mission phases and ConOps (Section 3.), the trajectory designed to reach Mars (Section 4.) and all the architectures employed during the mission: the cruise stage (Section 5.), the entry capsule (Section 6.) and the rover (Section 7.).

2. Landing and mining site selection

The selection of the landing site for MARS-PENGUIN mission is strictly constrained by its objectives. Indeed, the mission shall sample the geysers ejecta and the sub-glacial lake region, that was detected by MARSIS, an instrument on the Mars Express orbiter [1].

For this delicate operation, two possible strategies have been considered: landing in the lake area and then move to the closest geyser site or vice versa. In order to grant a safe landing, the following requirements for the site selection have been pointed out:

- be a planar region (slopes no steeper than 10°)
- be bare of cliffs or jagged peaks
- have a low density of rocks of relevant sizes

Based on the listed requirements and the following considerations, the option of landing firstly in the lake region has been selected.

First of all, the main goal of the mission is to analyse the lake region, while the geyser investigation is a secondary objective. Therefore, it would be better to reach the lake site firstly, since some fails may occur during the transfer geysers-lake, leading to a failure.

Besides, the lake region is very flat, while in the geyser site the presence of more irregularities is foreseen because of these explosive phenomena. Moreover, a geyser eruption may occur during landing. Of course, it may be possible to land a bit far from the geyser area, but still this region presents more uncertainties and this additional distance should be covered by the ground vehicle.

An analysis of the landing region has shown that there will not be issues with steep slopes, big rocks and great amount of dust. This has been confirmed from the albedo spectrum studies carried out in the South pole region, that indicate a predominant presence of material with high thermal inertia, excluding a high quantity of dust [2].

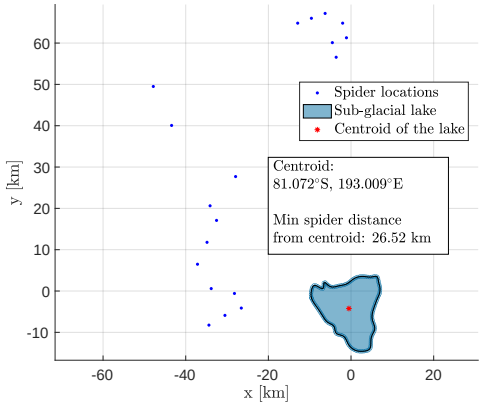

Fig. 1: Sub-glacial lake region and closer geysers.

Given the choice to land firstly in the lake region, an analysis of the images taken by MARSIS has been carried out, to find out the closest geyser sites. For this study, the lake geometry has been reconstructed by means of the WebPlotDigitizer software, [3] which allows to perform data points extraction from images. The image of the lake was taken from [1]. Using Haversine formula, the

distance between the centroid of the lake and the nearest spider site has been computed as 26.52 km. From the analysis, it has emerged that any point within the lake's area (that extends for 191.8 km^2), will be at a distance lower than 30 km from at least one spider (Figure 1).

2.1 Geysers

Since their identifications and for almost two decades, the geyser phenomena and the subsequent formation of the araineform terrains (denoted also spiders) have been studied. One of the main objectives of the MARS-PENGUIN mission is to deepen the knowledge of the geyser phenomenon as well as to confirm the studies done so far.

Geysers are seasonal events occurring in the early of southern spring. They form in the *cryptic* region of the South pole. Due to the condition of the latter, part of the ice condenses into the form of slab which is composed of larger grained solid CO_2 (polycrystalline ice), that is mostly transparent to visible light and opaque to the thermal infrared spectrum [4]. The layer of CO_2 ice performs a self-cleaning activity becoming transparent as the dust particles embedded in it migrate to the ground as a consequence of heating by solar radiation. Thus, when on ground, the basal sublimation at the bottom of the slab starts with a fast increase of pressure between the ice and the ground [5]. The gas enters and pressurises the porous substrate, until it increases leading to the slab's ruptures in its weakest point and so to gas jetting activity. Therefore, the gas escapes from substrate, entraining material at the substrate-free space boundary that produces the spiders [4]. The entrained material is lifted through the forced opening in the ice, forming an atmospheric plume. Material inside it can be transported downwind before settling on the surface, forming fan-shaped deposits [6].

2.1.1 The nearest geyser to the landing site

The condition of the presence of geyser in a region and consequently the formation of the spiders, depends on the soil's permeability, cohesion and porosity. The nearest geyser sites to the sub-glacial lake have various thin araineform terrains, as shown in Figure 2. They are characterised by rough central pits which usually have irregular shapes and radially organised dendritic troughs. Sometimes they are connected by troughs, which make it hard to count and distinguish them. Generally, thin spiders have an extension that goes from 50 to 500 m, with maximum trough width of 3 to 7 m and depth ranging from 0.6 to 2 m. Under the consideration of [7], the nearest spider's shape is characterised by an underlying soil that has:

- Low permeability such that restricts the gas flow causing a faster rise of local pressure. Sufficient pressure could be accumulated over a shorter distance to initiate gas jetting. Thus, it possibly leads to reduced spacing of spiders;
- High porosity of the substrate indicates higher capacity of containing sublimating CO_2 gas;
- High cohesion overlying soil determines the thin spider shapes with long dendritic structures.

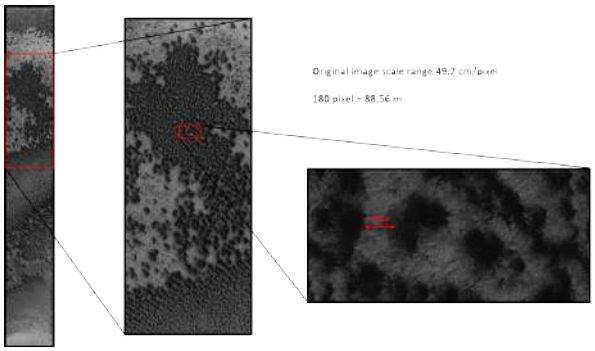

Fig. 2: The nearest thin geyser, centred approximately at 189.217° E and 80.687° S. HiRISE image: ESP_056553_0990 was acquired at L_s = 233.8° with 49.2 cmpx.

3. Mission Architecture

To satisfy the objectives of the MARS-PENGUIN mission a trade off was conducted via criteria matrix to select the best combination between: single/double launch, existing relay/proprietary orbiter and rover/hopper/both. The selected architecture includes a cruise stage, a descent module and a rover (Figure 4) The mission will also include a secondary aerial vehicle (Figure 3), contributing a lot in terms of demonstration and scientific return. This choice is made possible also by the absence of an orbiter and the resulting savings in mass. It is considered that the helicopter is placed inside the rover and it is detached when the rover reaches geysers location to observe them better.

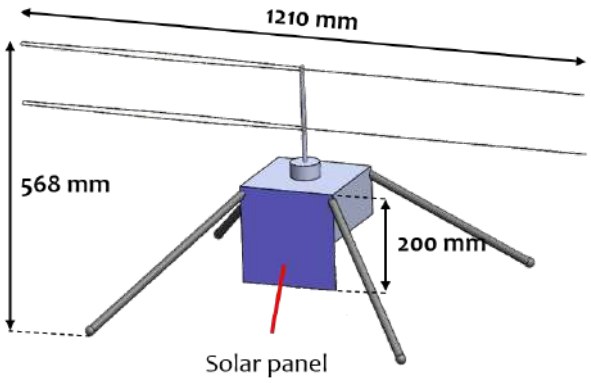

Fig. 3: MARS PENGUIN aerial vehicle

The preliminary mass obtained for this architecture, com-

puted with statistical method is of 2281 kg.

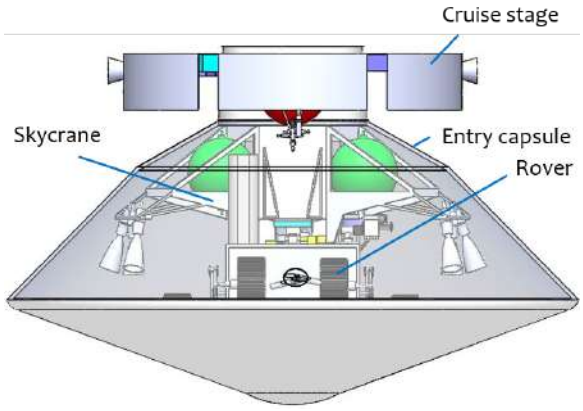

Fig. 4: Overall spacecraft configuration

Each component of the spacecraft is specialized in the next sections. The power budget of the mission is presented in Figures 5 - 7. One can notice the elevated Robotics power load at EDL caused by the separation and deployment pyro-devices (evidenced by a star in Figure 6). A significant contribution for the rover is introduced by the drill and locomotion. Skippers total power budget is 370 W including the margin of 12%.

Fig. 5: Power budget in Cruise.

Fig. 6: Power budget in EDL.

Fig. 7: Skipper's Power budget.

Based on the analysis performed from all the subsystems a mass budget has been performed for each segment of the mission. The criterion for margins at subsystem level has been reported in the following:

- 20% *Margin* if the related technology is well known and already space proven;
- 10% *Margin* if the related technology is not well known and already space proven.

Then 20% margin have been applied to each system, except for the cruise stage since it has been considered as a service module therefore another 20% margin have been applied to the overall system (275.37 kg). Hence, the resulting launch mass is ≈ 1807 kg with an Launch Vehicle Adapter (LVA) of 155 kg. The difference between the launch mass and the maximum P/L mass of the launcher selected, is 2743 kg. Hence, the difference is not 20% less than the launcher capability.

In Figure 8 are reported the mass for each segment with margin at subsystem level.

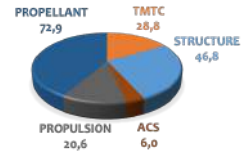

Cruise stage

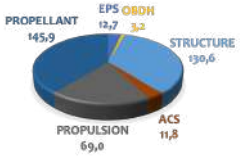

Skycrane

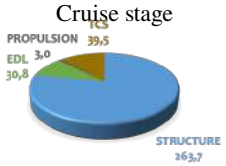

Entry Capsule

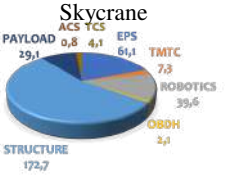

(d) Rover

Fig. 8: Mass division of each subsystem for segment.

3.1 Phases & ConOps

Given the long duration of the mission, a timeline with the different phases of the mission has been sketched and is reported in Figure 9. The timeline shows the duration of the mission in months and the two main segments of the mission: space and ground. The space segments starts when the spacecraft is released by the launcher on its interplanetary trajectory, while ground operations starts at the beginning of the descent phase on Mars.

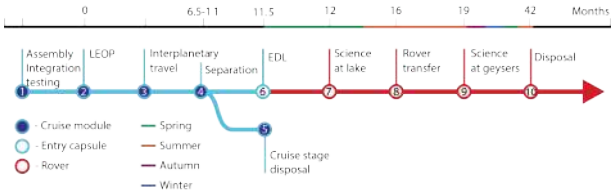

Fig. 9: Timeline of the mission. The seasons are relative to the southern hemisphere of Mars.

3.1.1 Assembly, Integration & Testing

Project integration and test: During this phase all the system is tested by performing functional and environmental testing. A full system validation is provided.

Launch Integration: here the integration phase can by repeated in a launch-integrated configuration.

3.1.2 Launch & Early Orbit Phase (LEOP)

Launch: from the launch countdown, until orbit injection. During the launcher ascension the spacecraft should remain "silent". Obviously, the power supply, data handling and thermal control systems must be active at some level during all phases and the whole mission duration. The main drivers are to withstand vibration and acceleration loads present into the path of the launcher through the Earth atmosphere. A strong ambient pressure decompression takes place.
Deployment: After detachment from the launcher the spacecraft should be brought in operational mode by activating the the corresponding subsystems. Then detumbling and telemetry exchange sequence must be performed. As a final step, a trajectory correction may be executed if needed. The spacecraft will start to be subjected to radiation coming from sun and space during the whole mission. It is important to maintain required attitude for communication and propulsive manoeuvres. Critical events like antenna deployment will take place.

3.1.3 Interplanetary travel & Separation

After LEOP the spacecraft is travelling towards Mars. Only telemetry exchange and trajectory corrections will occur. The major difficulties linked to the space environment are space and solar radiation, so consequently, the thermal control. Here the separation of the ground segment from the cruise stage takes place. A final TCM could happen before separation. The drivers are the reliability of the separation technique and the proper functioning of the separated segments.

3.1.4 Entry Descent & Landing (EDL)

The ground vehicle must be safely deployed to the Martian surface without sustaining any damage. All possible solutions include the deployment of parachutes after the velocity of the capsule has been partially slowed down by means of friction (the presence of an heat shield is crucial). The final descend might be performed by means of a sky crane or retrorockets and airbags. This phase will be monitored on Earth by the communication of the descent module with a relay orbiter around Mars.

3.1.5 Ground Operations

Science operations in lake region: once the rover has landed, it can begin working as intended, after all the system checks have been performed. It will need to perform sample collection of the icy soil in at least 5 different locations of the sub-glacial lake region.
Rover transfer: a crucial part of the MARS-PENGUIN mission is the rover journey from the sub-glacial lake region to the geysers site. The transfer will be performed during summer in order to exploit the solar illumination for guidance and to have less harsh conditions in terms of temperature and CO_2 ice on the surface.
Science operations at the geyser site: once the geyser site has been reached, the rover should start taking images in order to observe any geyser explosion from a safe distance. Once the explosion is occurred, the rover shall get closer to the geyser to sample and analyse the ejecta particles.
Non-nominal conditions: the ground vehicle must be able to withstand non-nominal conditions and also eventual failures. Custom-tailored modes are to be developed for these situations, in order not to compromise the whole mission, if not for a small period of time.

3.1.6 Disposal

Disposal occurs at the end of the life cycle of the mission. It should provide a safe decommissioning of the ground vehicle, but also of the cruise stage and of other potential parts (sky crane, parachutes...) according to COSPAR's planetary protection policy [8].
Based on the phases defined, here are reported the Concept of Operations (ConOps) of the overall mission shown in Figure 10.

(a)

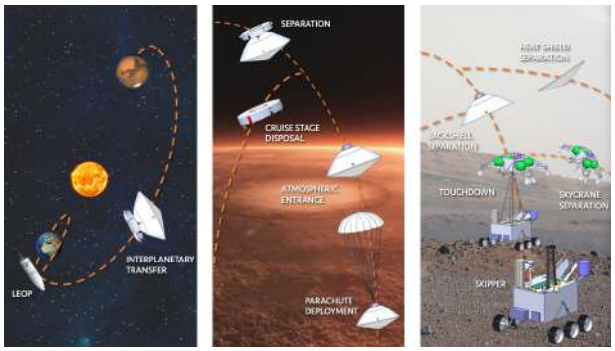

(b)

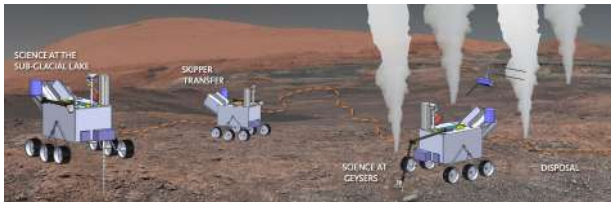

Fig. 10: ConOps from transfer to disposal of each segment.

4. Mission Analysis

This section briefly describes the mission analysis results, from the tradeoff process to the final trajectory. All the

calculation were performed using MATLAB.

4.1 Preliminary trajectory

The process of trade-off is schematised in Figure 11.

Fig. 11: Trajectory trade-off process

Through a 2024-2030 porkchop, taking into account the low TRL of some hardware and software to be employed, it has been decided to depart in 2028. Gathering also the constraints coming from the launcher it has been proceeded targeting the B-plane to fly-by Mars passing through the South Pole zone. Trajectory data retrieved from this computation have been used to feed an optimiser to obtain the final trajectory.

The possibility of exploiting a low thrust trajectory has been discarded due to long time of flight (TOF) and the additional power and mass required for an electric motor. To give a benchmark for Earth-Mars transfers, typical TOFs retrieved from the analysis carried out in [9] lie in the range from 600 to 1000 days. The decision of 2028 was based on the low TRL of some components, such as a European MM-RTG and an improved Rover GNC system that in turn led to discarding the other available trajectory with departure in 2026. The choice of the 2028 trajectory also meets the preferable condition of absence of CO_2 ice on the surface at arrival, a condition that verifies during the Mars South Pole spring.

4.2 Final trajectory

To obtain accurate parameters to set the boundary conditions of the optimisation process, it has been chosen to target the B-Plane. The algorithm firstly solves for the minimum ΔV using a patched-conic two-body Lambert solution for the transfer trajectory from Earth to Mars. Using this solution as initial guess, the second part implements a simple shooting method that attempts to optimise the characteristics of the geocentric injection hyperbola while numerically integrating the spacecraft's geocentric and heliocentric equations of motion and targeting components of the B-plane relative to Mars. The script optimises the overall ΔV.

The interplanetary injection has been supposed to occur impulsively from a circular parking orbit at an altitude of 200 km. Coordinates of the Sun, Moon and planets have been computed using DE421 JPL ephemeris.

Dates retrieved from the porkchop computation have been employed for this routine. In particular, the departure date has been set to 19/11/2028 as initial guess and allowed to vary within a symmetric interval of 60 days. The arrival date, which shall preferably fall in the martian spring time window, has been set to 15/09/2029 and allowed to vary on a symmetric interval of 30 days. The value of the **B** vector has been set in order to target an altitude above Mars of 150 km, a limit value retrieved by a preliminary EDL analysis. The results of this targeting allowed to obtain some boundary conditions to feed the optimizer, which was aimed to minimize the cost of the Trajectory Correction Manoeuvres (TCMs) to be performed.

The final trajectory data are here reported. In Table 1 the parameters of the departure hyperbola, obtained considering only J2 as a perturbation, are shown. It is worth to notice the C_3 of 9.436 km/s, compatible with most of the launchers capabilities and the launch date fixed at the end of November 2028.

Table 1: Departure hyperbola data

Parameter	Value	Units
UTC Date	23/11/2028 03:58:00	
C_3	9.436	km^2/s^2
Asymptote α	187.63	°
Asymptote δ	25.03	°

The spacecraft will depart from the Earth SOI on 26/11/2028 and will arrive at Mars after 297 days of cruise, on 19/09/2028. During the cruise it will perform two TCMs. The first will take place at the exit of Earth SOI and will require 25 m/s, while the second one will correct the trajectory before entering Mars SOI with a 63.5 m/s burn. The overall trajectory is shown in Figure 12.

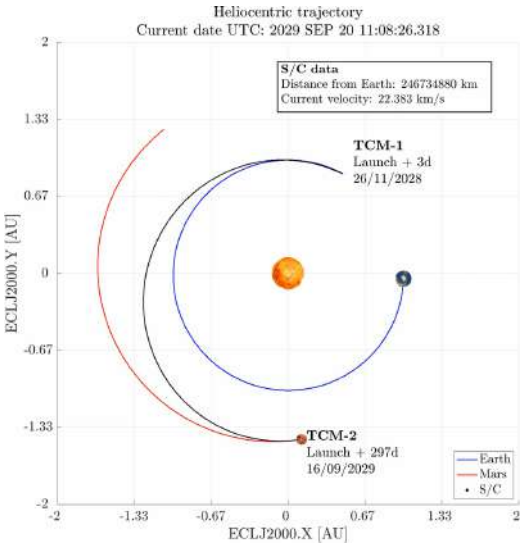

Fig. 12: Heliocentric trajectory in J2000 frame

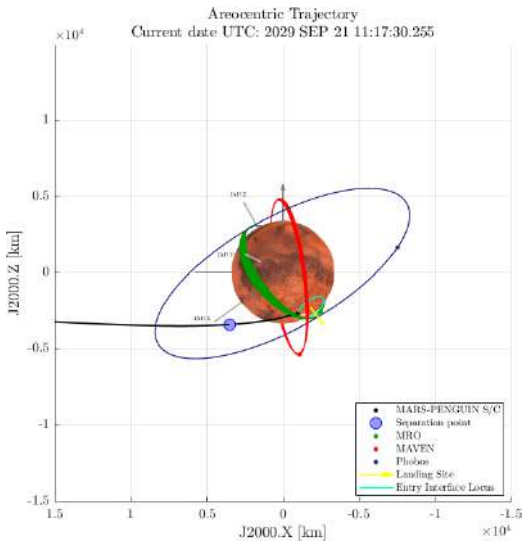

Fig. 13: Areocentric trajectory

The arrival hyperbola has been computed through a backward propagation process, starting from the entry interface point of interest. The optimal point has been identified among the ones of a circular cap at an altitude of 125 km from Mars surface and at a distance from the lake (measured on the Mars surface) of 473.5 km. The axis of the Equatorial reference frame (IAU Mars) have been retrieved at each epoch from the `.pcm` files provided by the NASA's Navigation and Ancillary Information Facility (NAIF). Concerning artificial satellites motion, MAVEN and MRO have been taken in account since they are the two candidates to serve as a relay for the communications. In Figure 13 the trajectory of the S/C in proximity of Mars is shown. It can be noticed that, about 15 minutes before the arrival at the entry interface, the aeroshell separates from the cruise stage along a direction parallel to the entry one with a relative velocity of 5 m/s. The optimal arrival point is reached by the aeroshell on 21/09/2029 with a velocity of 5.75 km/s and a flight path angle of $-12°$, as required for an optimal EDL phase.

5. Cruise stage

In this section the architecture of the cruise stage is described. Its configuration and all the subsystems operating during the interplanetary travel are hereby characterized.

5.1 Configuration

The design of the cruise stage is mainly based on the dimensions of the tanks, of the launcher adapter and of the HGA, which has been positioned at the centre.
As it is shown in Figure 14 and Figure 4, the two tanks have been placed symmetrically and close to the thrusters, to reduce the length of the pipes. The two clusters of thrusters and the instruments have been distributed according to the attitude control system requirements.
The lateral vertical panels protect the systems inside the cruise stage from the space environment, mostly from the thermal point of view. Some gaps between the panels are left for instruments and are used as a way of saving mass.

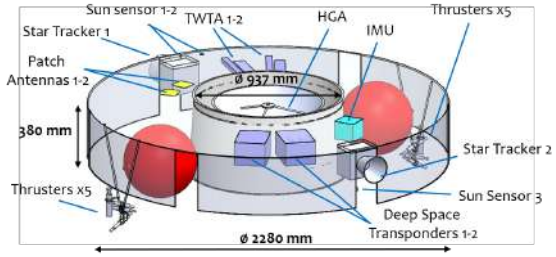

Fig. 14: Cruise stage preliminary design

5.2 Propulsion

The cruise stage propulsion system is composed of two clusters, each one with one MR-106L of 22 N thrust capability (primary propulsion) and four MR-103J thrusters of 1 N (secondary propulsion), all provided by Aerojet. The main engines are oriented in the axial direction of the cruise stage. For each manoeuvre the spacecraft will be re-oriented so that the thrust will have only an axial component. The secondary engine configuration allows to fully control the attitude of the cruise deck during all the interplanetary travel, with redundant thrusters for backup. Two rolling diaphragm tanks by MOOG, with 50.8 L capacity each, are filled with 72.93 kg of propellant (Hydrazine) and 0.116 kg of pressurising gas (Helium).
The two TCMs, as previously said, occur respectively 3 days after launch and at the entrance of Mars SOI (-3 from landing). The first TCM consumes 17 kg of propellant for a 10-minute manoeuvre of 25 m/s Δv. The second one, more demanding, lasts for 24 minutes in order to achieve 5.3 m/s Δv using thrusters at full capability and burns more than 40 kg of propellant (more than 50% of the propellant on board). Final propellant mass in the tank is not zero because part of the remaining propellant is used for AC manoeuvres (5.8 kg), whilst the other part can be used for unplanned TCMs. Since in a blowdown system the pressure in the tank gradually decreases while expelling propellant, it was verified that the feeding system could always provide the minimum feed pressure (5.9 bar) to the thruster accounting also for feeding and injection losses, in order to keep the thrusters working at nominal level.

5.3 ADCS

To design the architecture of the software and hardware in attitude and control subsystem, a thorough analysis on contributing source of perturbation for three phase of LEOP, cruise, and Mars approach has been performed. For the attitude determination, coarse and fine sun sensors

are combined with a star tracker to satisfy the requirements for pointing accuracy. An Inertial Measurement Unit is also equiped for providing angular velocity.

The selection of actuators for controlling the attitude of the cruise stage highly depends on the accuracy needed for each mode. The only frequent mode is the communication mode. Considering the thrusters allocated to perform the TCMs and also due to the fact that there is no solar panel to be pointed toward the Sun, it decided to use the same propulsion system used for TCMs, for the attitude manoeuvres. In Figure 15, the configuration of the thrusters is depicted.

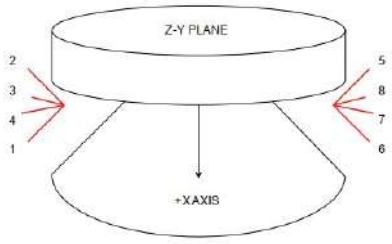

Fig. 15: Thrusters' configuration

5.4 *Thermal System*

A thermal analysis for the cruise stage has been done starting from a simple 3-node model of the worst hot (after departure with maximum solar flux $q = 1360$ W/m^2) and cold (before EDL when the solar flux is minimal $q = 590$ W/m^2) cases that this stage of the mission will encounter. The shell shall withstand the biggest temperature variations, whereas the internal nodes will be protected from the outside conditions, allowing smaller temperature gradients and variations.
The final architecture makes use of white paint surface finish, namely S13GP : 6N/LO-1 with $\varepsilon = 0.90$ and $\alpha = 0.18$, to keep the temperatures within the limits. The interplanetary leg is long enough for a small amount of degradation to be considered, but this is actually a positive factor for the mission, since the absorptivity will increase as the solar radiation will decrease, and the two effects will counteract each other.

6. Descent module

The descent module is composed of two segments: the skycrane and the entry capsule.

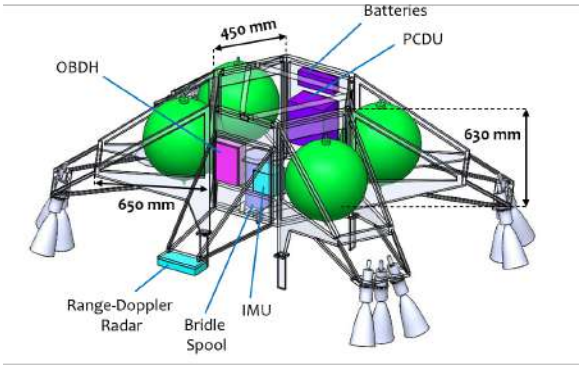

Fig. 16: Skycrane preliminary design

The central shape of the skycrane is hexagonal (Figure 16). This shape is particularly good for this element since 4 sides will be elongated to provide support to the thrusters and the other two opposite sides will be placed in correspondence of the RTG and of the drill which are the highest parts of the rover. A fifth smaller arm is used to place a radar-Doppler altimeter, that will be crucial during the descend phase. The skycrane will be attached to the rover by means of four legs.

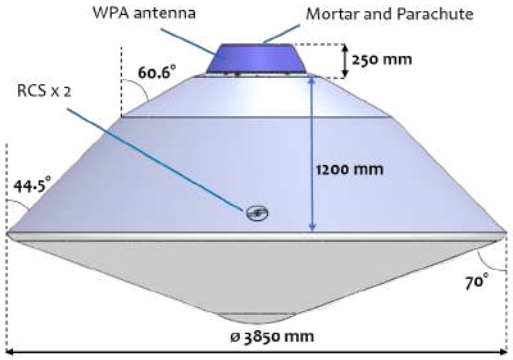

Fig. 17: Entry capsule preliminary design

The entry capsule is composed of the heat shield and the backshell. Its preliminary design is shown in Figure 17.
For the entry capsule the classical 70-degree half-angle sphere-cone shape used in almost all the other missions to Mars has been considered [10]. Its diameter has been set to 3.85 m according to the EDL analysis and its thickness has been defined with a thermal analysis (Section 6.3).
For the backshell, a triconic shape design has been selected. This shape is useful to have a larger diameter on the top of the capsule to grant enough space for the sky crane, but without having to enlarge too much the maximum diameter of the entry capsule. Its dimensions have been evaluated with a structural analysis (Section 6.4).

6.1 EDL

The EDL phase is one of the most critical parts of the whole mission.It has to safely deliver the rover to the Martian soil in three main sub-phases: entry, parachute deployment and landing. The main properties of the entry vehicle are collected in Table 2, whose design is the result of various mass, aerothermodynamic and trajectory tradeoffs.

Table 2: Characteristics of the entry vehicle

Entry vehicle	
Entry mass	1043.1 kg
Entry altitude	125 km
Entry velocity	5.749 km/s
Aeroshell hypersonic c_D	1.68
Aeroshell D	3.85 m
Ballistic coefficient	54 kg/m^2
Parachute c_D	0.65
Parachute D	16 m

6.1.1 Entry

A direct entry strategy has been selected, since the mission does not include a Mars orbiter. A ballistic kind of entry was analysed to understand the feasibility of this method, both in terms of landing effectiveness and precision. To model it, the entry vehicle was considered as a point mass entering with a 2D ballistic trajectory. An EFPA of $-12°$ has been selected from the results of a Monte Carlo analysis, as a tradeoff between achieving a narrower landing ellipse of uncertainty and guaranteeing a high enough deployment altitude. Indeed, the latter constraint may become a problem in the event of a relatively high elevation of the landing site, as for the mission (2.7 km). The entry properties corresponding to this choice of the EFPA are reported in Table 3.

Table 3: Parachute deployment properties (EFPA= $-12°$)

Parachute deployment conditions	
Deployment altitude	6.147 km
Deployment dynamic pressure	752 Pa
Deployment Mach number	1.51

6.1.2 Parachute

To better understand the dynamics of the parachute and capsule system, a model has been developed considering the whole as a double pendulum system, where the parachute and the capsule are modeled as point masses connected through two massless beams and a hinge. In correspondence of the latter a torsional spring is introduced to model the resistance to rotation opposed by the Kevlar suspension lines. As can be seen from Figure 18, the angle of attack of both the capsule and the parachute shows a very stable trend. This model allows to accurately estimate an aeroshell separation altitude of 5.77 km, as well as the horizontal and vertical velocity components at the backshell separation altitude (4.3 km): $v_h = 24.5$ m/s, $v_v = -59.4$ m/s.

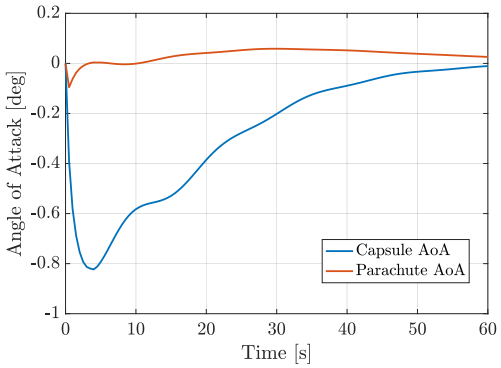

Fig. 18: Capsule-parachute double pendulum simulation

6.1.3 Landing

For the landing phase a model simulating the phases of a skycrane utilisation has been implemented. Starting from the values obtained by the parachute model at 1.6 km from the surface (4.3 km of altitude), the landing phase has been divided in 4 main phases:

1. Deceleration of the vertical velocity to 32 m/s and of the horizontal velocity to 0 m/s in the altitude range from 1600 to 145 m
2. Deceleration to a vertical velocity <1 m/s in the altitude range from 145 to 25 m
3. Constant velocity descent and rover release
4. Fly away of the skycrane

When the first phase starts the backshell and the heatshield have been already removed and the only remained masses are the one of the rover, deployed along a 8 m long bridle during the third phase, and of the skycrane.

Table 4: Relevant parameters of the landing phase

Phase	Thrust$_y$ [N]	Thrust$_x$ [N]	t_b [s]
1	2830.5	432	32.28
2	5228.5	0	7.6
3	1506.5	0	35.66
4	2230.6	500	11.42
t_b^{13}		75.54 s	
t_b^{tot}		86.96 s	
Skycrane impact distance		626 m	

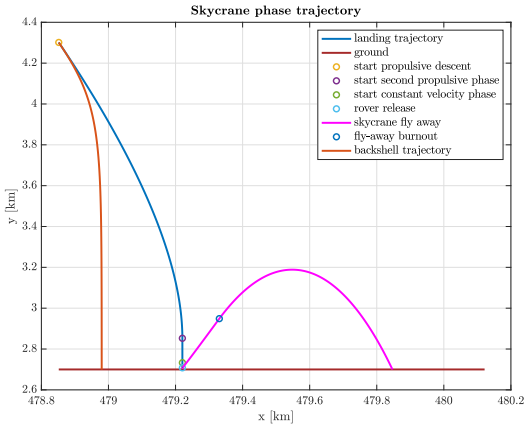

Fig. 19: Skycrane phase and backshell trajectory

Some calculations have been done to understand the uncertainty on the final landing position. For this purpose, a Montecarlo simulation has been performed considering the dynamic model previously described for the entry phase extended to a 3D case, with some additions in order to model the trajectory to reach the surface (Figure 20).

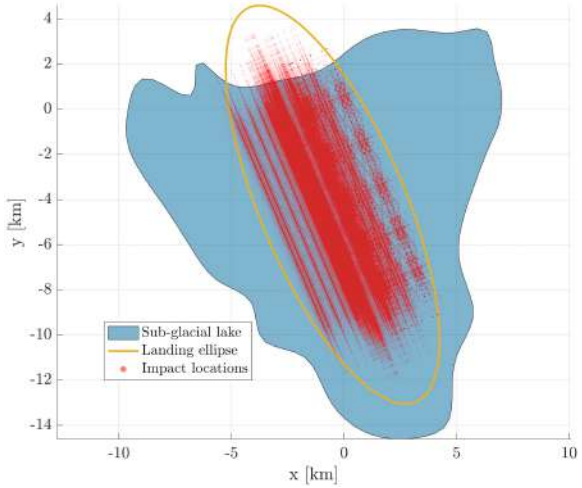

Fig. 20: Landing ellipse

The horizontal wind velocity effect has been modelled as well, considering the trend at the time and location of arrival [11]. Using the same dynamic model described for the Montecarlo analysis and considering a mean value of wind velocity of 93.81 m/s creating a lateral drag force, it comes out a maximum lateral deviation of 337.3 m, which can be corrected thanks to the skycrane propulsive system.

6.2 Propulsion

The propulsion system is centred in the skycrane with the tanks, but a set of RCS thrusters is located also in the backshell. They are four MR-106L of 22 N, same as the ones of the cruise stage, and are used for the beginning of EDL to stabilise the capsule when entering Mars' atmosphere. Twelve MR-104H throttling rocket engines, with 510 N nominal thrust but capable of reaching 554 N if used at maximum, are placed at the four corners of the skycrane structure. They will allow the skycrane to safely land Skipper on the surface. Four rolling diaphragm tanks (same of the cruise stage) will be filled with 148.85 kg of Hydrazine and 0.190 kg of Helium.

Since also an horizontal component of thrust is needed in some phases of the landing, the two lateral thrusters of each cluster are inclined of 20° in the XZ plane, whereas the central ones are aligned with the vertical axis. With respect to the XY plane, the lateral thrusters is inclined of 20° also in this direction, in order to have control on the y-axis too and counteract possible unexpected disturbances that could arise.

The entire configuration is shown in Figure 21.

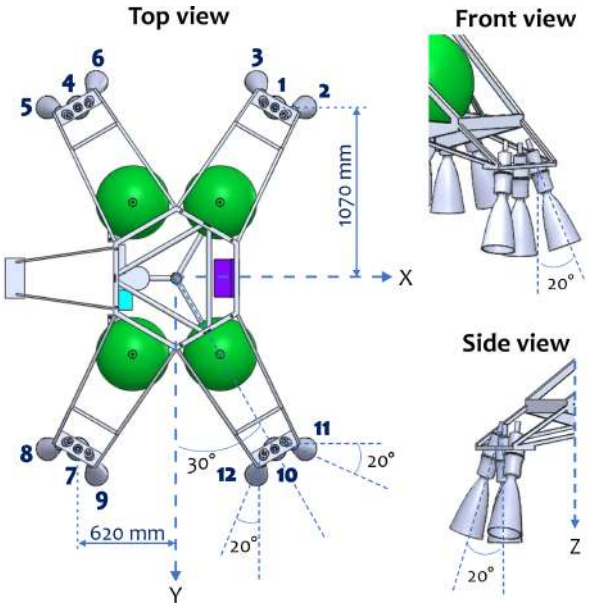

Fig. 21: Skycrane propulsion system configuration

As stated before, EDL is divided into four phases for what concerns the propulsive part: Phase 1 reduces to zero the horizontal velocity and to 32 m/s the vertical one, Phase 2 drastically brakes the landing stage till 0.75 m/s, Phase 3 is a constant velocity descent while lowering the rover, Phase 4 is the skycrane final burn to fly away from the rover and land at least 600 m distant from it.

The requested performance for the propulsive phase of the landing in terms of thrust and burning time is reported in Table 4. To allocate the requested thrust among the twelve thrusters, a constrained linear programming algorithm was used. Values of thrust required from each thruster obtained from it are reported visually in Figure 22 divided per thrusters and phases.

The system is robust not only with respect to the disturbances in x and y directions, but also to engine failures.

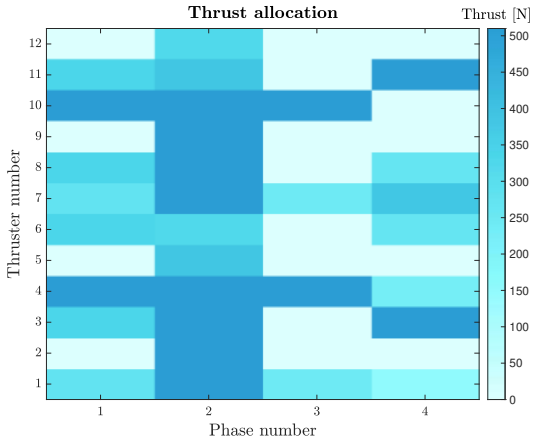

Fig. 22: Nominal thrust allocation

Indeed, the system is able to provide the same thrust profile even loosing of a lateral or central thruster for case of one engine failure or loosing two central engines. This proves that the system can ensure a safe landing even in the worst case of one-engine failure, which is the loss of a central engine during the most demanding phase in terms of vertical thrust required.

6.3 Thermal System

A thermal analysis for the EDL stage has been developed considering that the whole descent has similar heat fluxes during its entire duration. The only main difference is the friction, which relies on the speed and the composition of the atmosphere. Then, the temperatures for each part or component of the EDL phase has to be evaluated, in order to decide which nodes to select for the thermal problem. A net of 4 nodes has been employed to represent the most important components of the EDL phase: outside shell, equipment bay, batteries of the rover, processing of the skycrane, backshell. The shell node will be linked to the outside and to the other nodes. The nodes relative to the rover will be connected to the outside shell and to each other, and the backshell sensors node will only be connected to the outside shell node.
The highest temperature that is allowed to the structure is 250°, and this temperature is going to be considered as the temperature that the inner shell of the spacecraft has to deal with. The solution is to use a solar reflector. A white paint surface finish has been selected, namely S13GP : 6N/LO-1, with $\varepsilon = 0.90$ and $\alpha = 0.18$. The structure is made of aluminium honeycomb, which is able to keep the temperature low enough while having a low density and a width of 1.7 cm. The upper temperature margins are often very small, but since the EDL conditions do not change much throughout the whole process the temperature inside the shell is not expected to exceed 240°, while the rover equipment maximum temperature could reach 60°.

6.4 Structures

For the entry capsule Aluminium Honeycomb HexWeb CRIII 5052 Hexagonal and Aluminium 7075-T73 as skin material have been selected. The sandwich material is made of rigid panels of minimum weight which have aerodynamic smooth surfaces, high fatigue resistance and maintain corrosion protection at elevated temperatures.
The capsule has been at first sized for the launch phase, since it it is the driving condition for its design. For the sizing a FEA has been performed by studying the static and dynamic response, as well as the buckling phenomenon. The results of the sizing are shown in Figure 23.

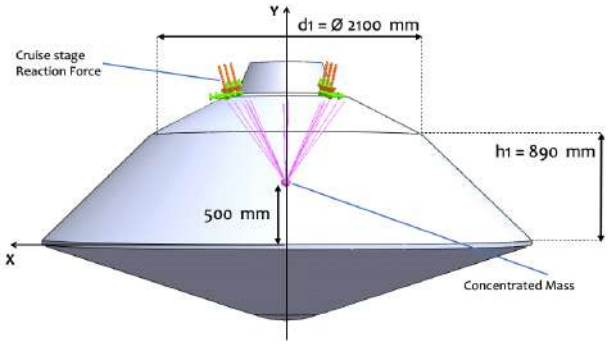

Fig. 23: Preliminary FEM analysis and sizing of the entry capsule during the launch phase

Furthermore, the high deceleration that acts on the entry capsule during the EDL phase has been considered to verify if the design of the structure.
The loading condition is the maximum deceleration (13.6 g), obtained from EDL phase study, and it acts only along the axial direction. As can be seen from the static analysis, under the loading condition the structure remains in the elastic field and buckling phenomenon do not occur. The strain field is represented in Figure 24.

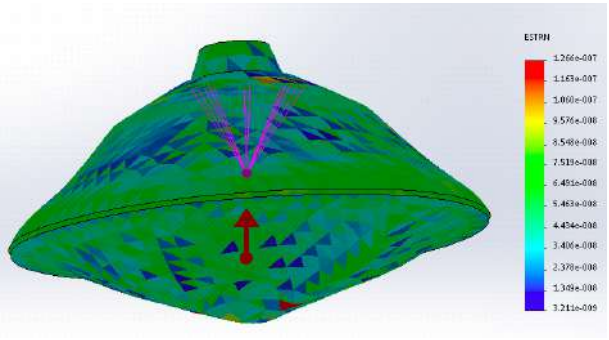

Fig. 24: Strain field under the maximum deceleration arising during the EDL phase

7. Rover

The rover has been the first element to be analysed. Indeed, its dimensions strongly constrain the sizing of the

descend module and of the spacecraft as a whole.
The dimensions of the main box have been selected to be compliant with the studies on the chassis and on the wheels reported in Section 7.5. The height of the box is a bit higher than usual to give more stability to the drill which is a very tall instrument. It has been divided into two main sections: a "scientific module" and a "service module". In Figure 25 and Figure 26, the rover Skipper is shown along with its dimensions and the positions of the different payloads and elements.

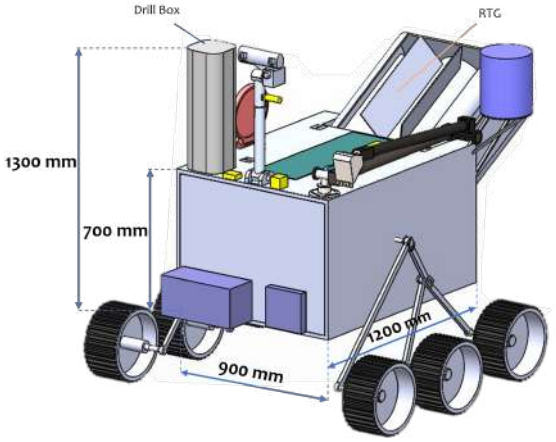

Fig. 25: Rover preliminary exterior design with payloads

7.1 Scientific Module

The scientific laboratory is characterised by two sections: an upper zone with the electronic boxes of the instruments and a bottom part, that will be an ultra clean zone, with the actual laboratory for samples handling and analyses.
Two ways of sample handling have been considered: a linear or a circular pattern. The circular one with a carousel that gathers and transports samples has been chosen for many reasons (Figure 31). This mechanism is the one usually used in space so it has a higher TRL, it is more compact and bidirectional.
Regarding the drill, the possibility of placing it outside the rover and having a mechanism to rotate it horizontally has been evaluated. However, given the large dimensions of it (1.3 m long) and its way of collecting samples with brushes, it was judged to be more efficient if placed directly close to the carrousel in a vertical position and inside the rover to be more stable. The drill box will have a degree of freedom in the vertical direction, so that it can get closer to the ground.
The scoop will deliver its samples into a hole (that will be equipped with a closing mechanism) on the top of the rover. The samples in this case will be gathered in the crushing station, that will make the dimensions of the particles compatible with the requirements of the instruments, and then a dosing station will distribute samples to the collectors. Finally, a cleaning station has also been defined to properly clean the collectors from the previous samples.

7.2 Service Module

As already explained, the service module contains all the other elements necessary to support the scientific laboratory such as power, thermal control, on-board data system and telecommunication system.
The RTG is placed at the very back of the rover, in order to radiate the majority of its huge heat power in the external environment and not inside the rover. Instead of being horizontal, it is inclined of an angle of 60° for stability and mass distribution reasons. The other elements have been placed according to their specific requirements.

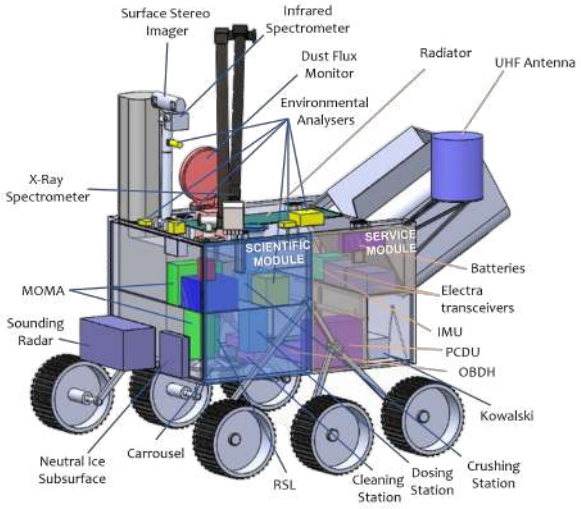

Fig. 26: Rover preliminary interior design with payloads

7.2.1 Helicopter positioning and release mechanism

Kowalski will be released once the geyser site region has been reached by the rover Skipper. Therefore, the helicopter shall be stowed within the rover for the whole journey from the lake region and a release mechanism should be proposed. To fit inside the rover, its legs and blades will be folded. The blades will be put on one side. The helicopter height is greater than the ground clearance, so it is not possible to release it directly below the rover. Therefore, the proposed solution is characterised by the release of part of the bottom and rear panels to let the helicopter deploy its legs, while still attached to the rover. Skipper would then release it and move away Figure 27.

7.3 Operational Modes

Once the mission phases and tasks have been properly outlined, the modes of the mission have to be defined.

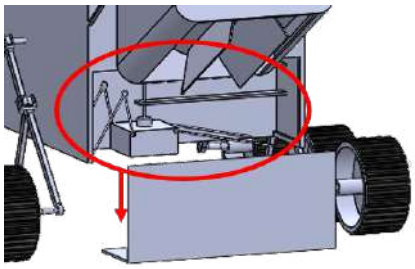

Fig. 27: Release mechanism of the helicopter

These modes, which are shown in the list below, should be seen as subroutines that have to be employed by the ground and space segment to overcome all the different scenarios that could occur in the mission, from simple tasks to non-nominal conditions:

- SLP - Sleep mode. Spacecraft or rover are switched off, minimum power, TCS still active
- STB - Standby mode. Active with minimum power, waiting for commands
- STE - Essential check mode. Diagnoses electrical equipment
- ATT - Attitude mode. Active during spacecraft attitude manoeuvres
- PRP - Propulsive mode. Active during in-space manoeuvres
- COM - Communication mode. Space and Mars segments use this mode to send or receive information
- EDL mode, Used in atmospheric entry to perform autonomous descent
- SAF - Safe mode. Decreases the impact of active faults shutting down all the systems at risk and works on solutions to the faults
- ROV - Roving mode. Moving on the Martian surface
- SCI - Science mode. Perform sampling and analysis of soil and geyser ejecta particles

Once all these modes have been defined, we can associate one or more of them to each phase of the mission as shown in Table 5, in order to have a more general idea of what is happening at every step of the mission.

Table 5: Possible modes during the mission

Phase	Possible modes
LEOP	SLP - COM - ATT - PRP - STE
Interplanetary travel	COM - ATT - PRP
Separation	COM - ATT - PRP
EDL	LAN - COM - ATT - PRP - STE
Ground oper.: lake	SLP - STB - COM - ROV - SCI
Ground oper.: transfer	STB - COM - ROV
Ground oper.: geysers	SLP - STB - COM - ROV - SCI
Disposal	SLP - STB

7.4 EPS

The main drivers for sizing and architecture definition of the Electric Power Subsystem (EPS) of the mission are:

1. the Rover should be able to operate below 80°S for at least 30 terrestrial months
2. be able to travel at least for 4 hours per sol

Study showed that ATT, PRP, EDL are the key modes in terms of power demand that will mostly affect the sizing process. Considering that they are used in Cruise and EDL and that the Rover consumption is much less, it is reasonable to introduce a separate power sources for each stage with a possibility of sharing the generated power at different phases. The minimal consumption in cruise phase is estimated 58.80 W in Sleep mode and 40.34 W for Skipper. These are due to the proper functioning of the TCS and OBDH watchdog timers. The maximum load of 1700 W is achieved during EDL by the separation and parachute deployment systems while performing energetic attitude manoeuvres. The major constraint to pay attention to when sizing Skipper's power source is its operation duration on Mars. It is requested to operate at least for 30 terrestrial months which corresponds to slightly more than one Martian year. It means that Skipper must survive the Martian south winter and the polar night whose duration is about 300 terrestrial days. The application of SA would require another source that should provide the power of 40.34 W during this period. The energy consumed through this time is estimated to be 290304 Wh using an electric heat source, and 14400 Wh using a radioisotope heater unit. It is highly unlikely to achieve this values using any sort of chemical batteries within a reasonable mass budget. Therefore a radioisotope electric power generator widely used in Mars missions will be considered. The stages will share the Main power bus and complement each other in order to charge the battery or satisfy a high power demand. Shut-off switches are foreseen to disconnect the circuits before the separation of the stages. The Mars Penguin mission EPS architecture is presented in Figure 28.

7.5 Locomotion subsystem sizing

The locomotion subsystem of the rover has been studied in terms of wheels number and suspension system.
The wheel sizing will determine the traction capability of the rover. The real design of the wheel may complicate the calculation process so additional testing is preferable.There are three general indices of performance to consider for the locomotion system design:

- Trafficability, which is a robot's ability to traverse soft soils or hard ground without loss of traction.
- Maneuverability, which addresses a robot's ability to

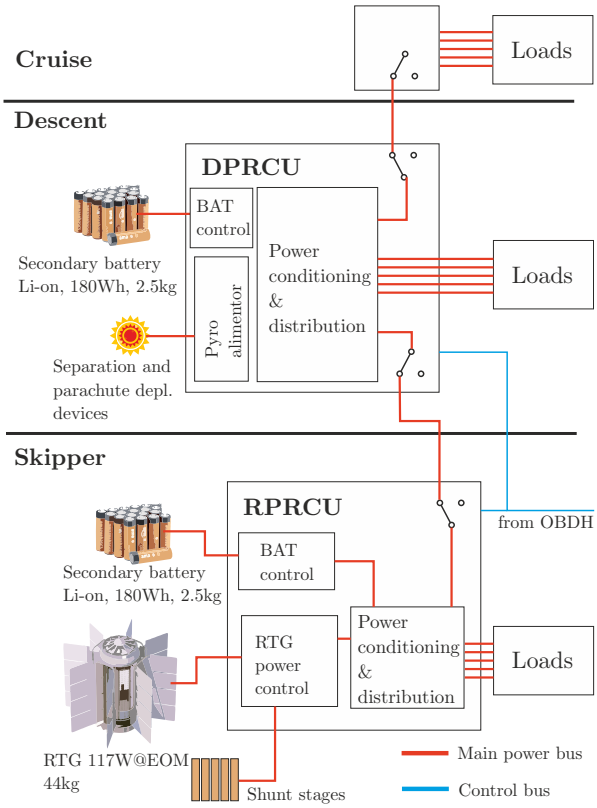

Fig. 28: Mars Penguin mission EPS architecture

navigate through an environment.

- Terrainability, which captures a robot's ability to negotiate terrain irregularities.

The trafficability aspect has been mainly considered at this stage of the design. Bekker's Theory proposed in [12] and the model used [13] have been employed.
The main performance parameters are summarised in Table 6, comparing 4-wheel and 6-wheel configurations with rigid suspension (worst-case choice), both considering 1 cm high grousers and only front wheels powered. For the 4-wheel configuration diameter and width of the wheels are 37 cm and 25 cm respectively; instead for the 6-wheel configuration dimensions are 35 cm and 16 cm.

The 4-wheel rover is advantageous in terms of soil thrust, while the 6-wheel configuration leads to better results regarding all the other parameters: smaller dimensions, lower motion resistance and higher maximum slope and lower drive power. Considered that 6 wheels are also much more convenient in terms of manoeuvrability and overcoming obstacles, this configuration has been selected for Skipper.
The suspension system chosen for Skipper is the rocker-bogie configuration, since a long travel has to be performed from the sub-glacial lake to the geyser sites. This type of configuration is the best one for optimal stability

Table 6: Summary of the expected trafficability of 4-wheel and 6-wheel configurations with rigid suspension on flat terrain. For the input power: drivetrain efficiency: 0.7, motor efficiency: 0.8, drive electronics efficiency: 0.85.

Performance metric	Unit	4-Wheel	6-Wheel
Rover Drawbar Pull	N	~ 450	~ 450
Travelling speed	m/s	0.1	0.1
Sinkage	cm	2.03	2.10
Maximum slope	deg	13.60	13.60
Drawbar Pull/wheel	N	112.73	75.09
Total Resistance/wheel	N	221.87	150.42
Soil Thrust/wheel	N	334.60	225.52
Drive Torque/wheel	Nm	41.05	26.32
Drive Power/wheel (Outpt)	W	22.19	15.04
Drive Power/wheel (Input)	W	93.22	63.20
Total Drive Power	W	186.44	126.40

and control to traverse on uneven terrain for the following reasons [14]:

- it does not need for axles and springs, which are usually susceptible to dust accumulation in the Mars harsh environmental conditions;
- it allows the rover to travel over steps up to two times the wheel diameter;
- during the motion it maintains centre of gravity of entire vehicle: when one rocker moves upward then the other goes down through a differential mechanism that connects the left and right side rocker bogie assemblies, which helps to minimise the maximum or average ground pressure;
- each of the wheels is powered individually by its own DC-motor and the presence of the differential mechanism allows a balanced spreading of the load between wheels and motors;
- it allows each of the six wheels to remain in contact with the ground while it traverses over obstacles, helping to propel the vehicle over the terrain.

7.6 Sub-glacial lake and geysers sampling

Skipper shall collect samples when it is above the sub-glacial lake. The selection of the areas to penetrate will be made by the scientists who will have available orbital images and the Surface Stereo Imager (SSI) on rover and helicopter cameras. Scientific payloads such as Sounding Radar and Neutral Ice Subsurface will be also used.
A drill was selected as the best option to obtain samples. It has to be designed as an icy soil drill and, based on the reference drills, the estimated mass and power (without margins), are 20 kg and 100 W. Rico, which is the name given to the drill, shall be able to dig at least 1 m under the Martian surface, and the total length shall not exceed 1.3 m, in order to keep it in a vertical position inside the rover body. Considering these dimensions, multi-rod technology is not required. The box containing the drill

must be able to move down from the body of the rover in order to use the entire length of the auger to drill the ground. The possible configuration is shown in Figure 29.
Once in the Geyeser region, the MARS-PENGUIN mission shall first of all observe the phenomenon of the eruptions and record it with the SSI on the Skipper rover, and the camera on Kowalski, the helicopter. A Robotic Arm (RA) was selected for MARS-PENGUIN mission and the RA of Phoenix mission [15], with 4 DoF and a back-hoe design, can be considered as a first baseline for MARS-PENGUIN RA, especially for the scoop design.
A possible prototype of the MARS-PENGUIN's robotic arm, baptised "Soldato", is shown in Figure 30. The RA is composed by five parts: a base, a shoulder pitch joint, an upper arm, a forearm and a scoop. The upper arm and the forearm are both 0.9 m long and, extended to its limit, the arm can reach a point 2 m far from the base. The scoop capacity is 731.15 cm^3. The instrument is also equipped with an X-Ray Spectrometer to select the optimal sampling site.

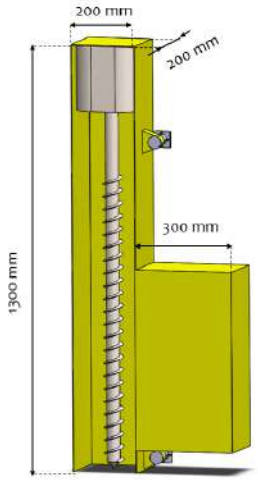

Fig. 29: Possible configuration for the drill Rico

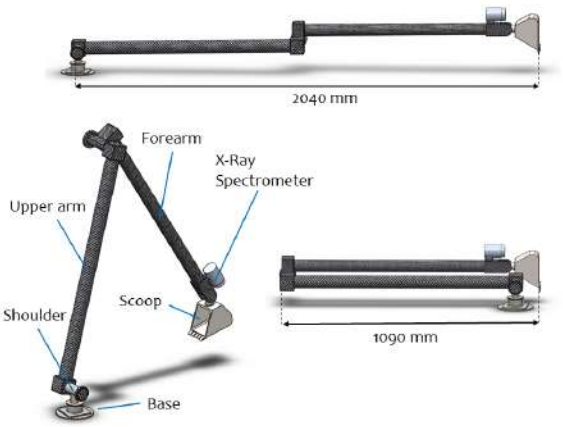

Fig. 30: Soldato in different positions

7.6.1 *Sample handling and analysis*

Skipper is equipped with a sample analysis laboratory, which includes the Mass Spectrometer and the Raman Laser Spectrometer (RLS) for sample in-situ analyses. The rover will need a system for the material handling and transfer to the above mentioned laboratory. This will be the assembly of structures, mechanisms, containers and devices that allow transport and processing of the samples collected by the two sampling instruments.
The rover shall be provided with at least 10 containers to collect the material from the drill, in order to guarantee the 5 samples required with a certain margin.
Concerning the geyser sampling instead, after collecting the samples from the ground, the robotic arm shall place the material in a dedicated storage area in the rover from which the sample is transferred to the laboratory.

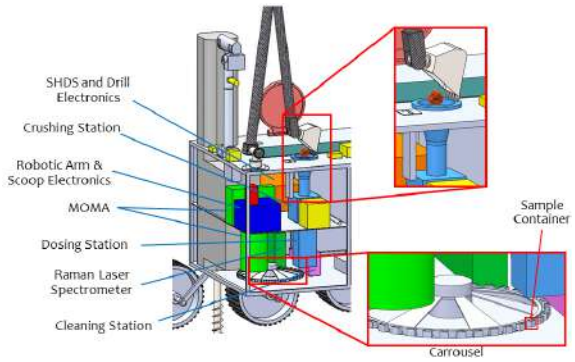

Fig. 31: Skipper Sample Handling and Distribution System

7.7 *Telemetry & Telecommand*

The rover will have no direct-to-Earth communication capability and will rely exclusively on UHF relay links.
The polar location of the landing site will on the one hand result in limited LoS with Earth, on the other hand it will further promote the use of a relay link. Indeed, Mars orbiters are typically placed in near-polar orbits, which means they cross both polar regions once per orbit, thus resulting in increased contact frequency compared to lower latitudes.
Among the currently operating orbiters of the Mars relay network, MRO has been identified as the most suitable choice. It is currently estimated that MRO will have enough propellant to keep operating into the 2030s.
For both TX/RX, BPSK modulation[1] + (7, 1/2) convolutional coding have been chosen. MRO's Electra payload is provided with a UHF LGA antenna with 5 W RF output power in full duplex mode. The radiation pattern reported in [16] has been used in simulations. The rover will be equipped with a redundant Electra-lite transceiver [17] delivering 8.5 W of RF output power. This communication

[1]which is the only kind supported by MRO's proximity link

payload weighs 3 kg and requires 65 W of input power.
A quadrifilar helix antenna design has been chosen for the RUHF, given its extremely wide beam and acceptable gain even at very low elevation angles.
The Electra payload features adaptive data rate, which allows it to adjust the data rate along any orbiter pass. In particular, as MRO approaches the nadir direction, the SNR tends to increase (i.e. higher data rates are allowed). Accounting for the fact that all powers of 2 in the range from 2 to 2048 kbit/s are supported by the return link to MRO and considering a $\mathrm{BER}_{\max} = 10^{-5}$ along with a 3 dB link margin, the dependence of the resulting maximum allowed data rate as a function of the orbiter elevation can be easily obtained. We may at this point determine the data return profile by propagating MRO's orbit and considering the previous dependence. The result of the overall simulation is reported in Figure 32.

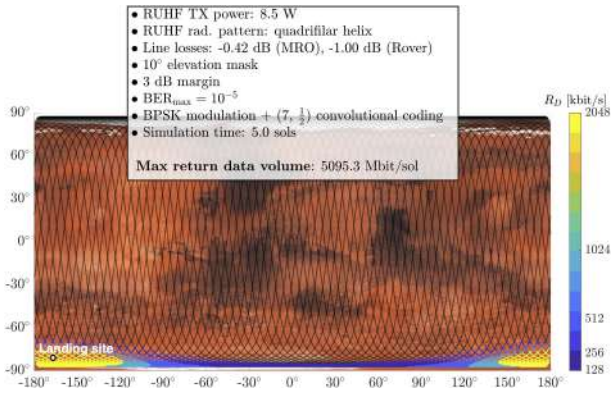

Fig. 32: Data return performance depending on orbiter pass ground track

It has to be underlined that, although by assuming to exploit all pass opportunities a maximum data volume return of 5.1 Gb/sol would be achieved, such a value actually overshoots the maximum allocated space on Solid-State Recorders of up to 5 Gbit/day for all landed elements at Mars relying on MRO. In addition to this, in a more realistic scenario one would be able to relay data to an orbiter only during a limited portion of the day, since the rest would be devoted to science operations and/or roving.
Assuming to exploit just the N best successive pass opportunities during a given sol, the average return data volume would be 1214, 1696.1 and 2083.4 Mbit/sol, in correspondence of $N = 2, 3, 4$ respectively.

8. Conclusions

In this paper the MARS PENGUIN space mission was presented. It is aimed to investigate the Southern polar cap and the geysers on Mars. After analyzing the baseline requirements and objectives for the mission is was found the final architecture, composed by an entry capsule, a skycrane, a rover and a small helicopter, with a low mass budget if compared to other missions. With this configuration and following a precise schedule, MARS PENGUIN mission is able to fulfil all the given objectives. The mission is expected to depart at the end of 2028 and reach Mars in the middle of 2029, during the martian south pole spring, when geysers are active. During the mission lifetime, sampling operations required will be carried out by a Rover with the support of a small Helicopter.
The goals to be met for the success of the mission require the implementation of some low TRL technologies, which are expected to be further developed in the upcoming years.
The most concerning one is the GNC capabilities for roving, which need to be improved in terms of autonomy and reliability. To proceed towards phase B there will be some refinement to be performed in the adopted models, such as parachute tumbling in EDL phase. Also, a better characterisation of the customised functions needed for drilling and sampling the peculiar soil at Southern Pole. Once overcome these criticalities, we are confident that a successful MARS PENGUIN mission will provide significant contributions to the discovery of water resources and eventual extraterrestrial life, paving the road for future Martian settlements.

References

[1] Roberto Orosei, Sebastian E Lauro, Elena Pettinelli, Andrea Cicchetti, Marcello Coradini, Barbara Cosciotti, Federico Di Paolo, Enrico Flamini, Elisabetta Mattei, Maurizio Pajola, et al. Radar evidence of subglacial liquid water on mars. *Science*, 361(6401):490–493, 2018.

[2] Philip R Christensen, Joshua L Bandfield, Vicky E Hamilton, Steve W Ruff, Hugh H Kieffer, Timothy N Titus, Michael C Malin, Richard V Morris, Melissa D Lane, RL Clark, et al. Mars global surveyor thermal emission spectrometer experiment: investigation description and surface science results. *Journal of Geophysical Research: Planets*, 106(E10):23823–23871, 2001.

[3] Ankit Rohatgi. WebPlotDigitizer.

[4] Jingyan Hao, GG Michael, Solmaz Adeli, and Ralf Jaumann. Araneiform terrain formation in angustus labyrinthus, mars. *Icarus*, 317:479–490, 2019.

[5] Antoine Pommerol, Ganna Portyankina, Nicolas Thomas, K-M Aye, CJ Hansen, M Vincendon, and Y Langevin. Evolution of south seasonal cap during martian spring: Insights from high-resolution observations by hirise and crism on mars reconnaissance orbiter. *Journal of Geophysical Research: Planets*, 116(E8), 2011.

[6] Sylvain Piqueux, Shane Byrne, and Mark I. Richardson. Sublimation of mars's southern seasonal co2 ice cap and the formation of spiders. *Journal of Geophysical Research: Planets*, 108(E8), 2003.

[7] J Hao, GG Michael, S Adeli, R Jaumann, G Portyankina, E Hauber, C Millot, and W Zuschneid. Variability of spider spatial configuration at the martian south pole. *Planetary and Space Science*, 185:104848, 2020.

[8] Gerhard Kminek and John D Rummel. Cospar's planetary protection policy. *Space Research Today*, 193:7–19, 2015.

[9] Wanmeng Zhou, Haiyang Li, Hua Wang, and Ran Ding. Low-thrust trajectory design using finite fourier series approximation of pseudoequinoctial elements. *International Journal of Aerospace Engineering*, 2019, 2019.

[10] Dinesh Prabhu and David Saunders. On heatshield shapes for mars entry capsules. In *50th AIAA Aerospace Sciences Meeting including the New Horizons Forum and Aerospace Exposition*, page 399, 2012.

[11] http://www-mars.lmd.jussieu.fr/mcd_python/, 2020.

[12] Mieczyslaw Gregory Bekker. Introduction to terrain-vehicle systems. part i: The terrain. part ii: The vehicle. Technical report, MICHIGAN UNIV ANN ARBOR, 1969.

[13] Dimitrios S Apostolopoulos. Analytical configuration of wheeled robotic locomotion. *The Robotics Institute of Carnegie Mellon University Technical Report CMU-RI-TR-01-08*, 2001.

[14] Thomas Brooks, Graham Gold, and Nick Sertic. Dark rover rocker-bogie optimization design. 2011.

[15] Robert Bonitz, Lori Shiraishi, Matthew Robinson, Joseph Carsten, Richard Volpe, Ashitey Trebi-Ollennu, Raymond E Arvidson, PC Chu, JJ Wilson, and KR Davis. The phoenix mars lander robotic arm. In *2009 IEEE Aerospace conference*, pages 1–12. IEEE, 2009.

[16] Jim Taylor, Dennis K Lee, and Shervin Shambayati. Mars reconnaissance orbiter. *Deep Space Communications*, page 193, 2016.

[17] L3Harris. Mars UHF Transreceiver.